IEEE Photonics Journal
An IEEE Photonics Society Publication

Open Access

16-Wavelength DFB Laser Array With High Channel-Spacing Uniformity Based on Equivalent Phase-Shift Technique

Volume 6, Number 6, December 2014

Yuechun Shi
Lianyan Li
Jilin Zheng
Yunshan Zhang
Bocang Qiu
Xiangfei Chen, Senior Member, IEEE

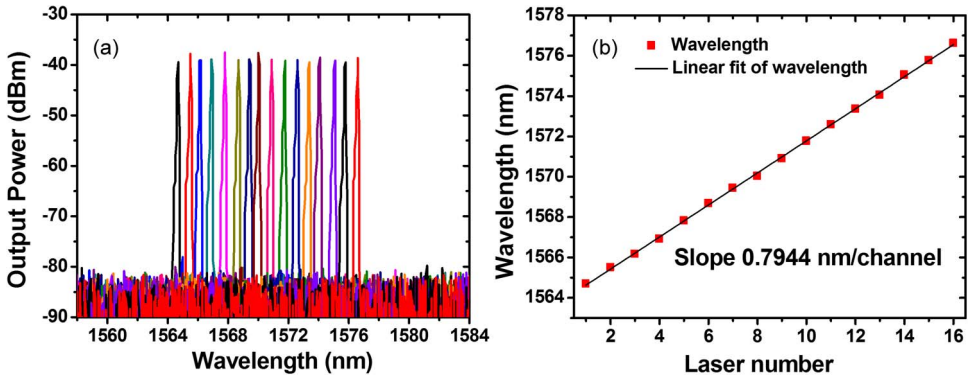

DOI: 10.1109/JPHOT.2014.2374610
1943-0655 © 2014 IEEE

IEEE photonics SOCIETY

IEEE

16-Wavelength DFB Laser Array With High Channel-Spacing Uniformity Based on Equivalent Phase-Shift Technique

Yuechun Shi,[1] Lianyan Li,[1,2] Jilin Zheng,[1,4] Yunshan Zhang,[1,5] Bocang Qiu,[3] and Xiangfei Chen,[1] *Senior Member, IEEE*

[1]Microwave Photonics Technology Laboratory, National Laboratory of Microstructures, and School of Engineering and Applied Sciences, Nanjing University, Nanjing 210093, China
[2]Photonics Research Group, Department of Information Technology (INTEC), Ghent University, 9000 Ghent, Belgium
[3]Suzhou Institute of Nano-Tech and Nano-Bionics, Chinese Academy of Sciences, Suzhou 215123, China
[4]Institute of Communication Engineering, PLA University of Science and Technology, Nanjing 210007, China
[5]Suzhou High-Tech Institute, Nanjing University, Suzhou 215123, China

DOI: 10.1109/JPHOT.2014.2374610

Manuscript received October 19, 2014; revised November 16, 2014; accepted November 18, 2014. Date of current version December 9, 2014. This work was supported in part by the National Natural Science Foundation of China under Grant 61090392 and Grant 60877043; by the National "863" Project under Grant 2011AA010300; by the Fundamental Research Funds for the Central Universities and PAPD, Jiangsu Province, China; by the Natural Science Foundation for the Youth under Grant 61306068; and by the Natural Science Foundation of Jiangsu Province of Youth under Grant BK20130585 and Grant BK20140414. Corresponding authors: Y. Zhang and X. Chen (e-mail: zys5014@163.com; chenxf@nju.edu.cn).

Abstract: The high accuracy of lasing wavelength spacing is one of the key requirements of a distributed feedback (DFB) semiconductor laser array. However, the nonuniformity of the wavelength spacing is increasingly deteriorating with the increase in the channel number in the laser array. In this paper, theoretical study was made to investigate the effects of sampling pattern deviation and seed grating, as well as waveguide dispersion on the wavelength-spacing uniformity for multiwavelength DFB semiconductor laser arrays (MLAs) fabricated using the reconstruction equivalent chirp (REC) technique. A simple measurement method of dispersion for DFB semiconductor lasers based on the REC technique is also proposed. With the dispersion compensation being included in the sampling period design and small deviation in the seed grating period being guaranteed, a high-channel-count (16-channel) DFB laser array with precise channel spacing of 0.7944 nm/channel (design value of 0.80 nm/channel) was achieved in our experiment. It shows excellent channel-spacing uniformity, and most wavelength residuals are within $\pm$0.10 nm.

Index Terms: Distributed feedback lasers, laser arrays, dispersive media, wavelength measurement.

1. Introduction

Multi-wavelength distributed feedback (DFB) semiconductor laser arrays (MLA) are the key components in the photonic integrated circuits (PICs) [1]–[5], and one of the most important parameters for MLAs is their wavelength spacing precision [1], [6]. With the rapid advances in network capacity, wavelength spacing becomes increasingly smaller in dense wavelength

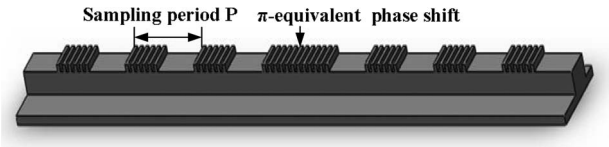

Fig. 1. Schematic of the DFB laser with π-equivalent phase shift.

division multiplexing (DWDM) systems, for example, the wavelength spacing reduces to 0.2 nm (25 GHz) from 0.4 nm (50 GHz), and in the meantime, the channel number increases as well. The increase in the channel number in an MLA has significant impact on production yield [1], as every channel has to meet the ITU-T standards. In order to obtain high precision of lasing wavelength spacing, both the grating period of each laser and the effective refractive index (ERI) of materials need to be precisely controlled. In addition, the complex structures such as phase shift and chirp are employed to ensure that all channels lase in single longitudinal mode (SLM). As a result, it is difficult to fabricate a DFB laser array with high channel spacing uniformity and good SLM property. Up to now, Electron Beam lithography (EBL) has been widely used for the grating fabrication. EBL can be used to write arbitrary grating lines, but it has drawbacks of long writing time, stitching error and some other issues [6], [7]. The Reconstruction-Equivalent-Chirp (REC) technique was first proposed to fabricate fiber Bragg grating laser [8] and then was proposed to fabricate DFB semiconductor lasers [9], [10]. It is a new approach to fabricate the complex grating patterns such as equivalent phase shift and chirp [11], [12]. With the REC technique, one can straightforwardly fabricate DFB laser arrays using standard holographic exposure and micrometer scale photo-lithography process which is low cost and has high grating pitch control. But with increase in channel count or wavelength coverage, the arrays processed using REC technique suffer from increasing non-uniformities due to waveguide dispersion, basic (seed) grating non-uniformity and sampling pattern errors. In order to achieve precise channel spacing with large channel count, some issues in REC technique such as seed grating uniformity, sampling pattern and waveguide dispersion have to be addressed. For an MLA with small wavelength coverage, the dispersion can be ignored as the error of lasing wavelength spacing arising from the dispersion can be easily compensated by an additional tuning. However when the wavelength coverage of an MLA is large enough, the wavelength error will be seriously accumulated one by one, resulting in significant mismatch between the actual and required lasing wavelengths if dispersion is incorrectly valuated or is not considered. Therefore, it is very important to compensate the waveguide dispersion by pre-designing the sampling pattern. For grating period, it is usual to have non-uniformity in wavelength spacing, particularly when the channel count is high. In this paper, the uniformity of wavelength spacing for laser array based on the REC technique is studied in detail, and a simple method to measure the dispersion is also proposed. With the dispersion compensation being included in sampling period design and small deviation in seed grating period being guaranteed, high channel count (16-channel) DFB laser array with precise channel spacing of 0.7944 nm/channel (design value of 0.80 nm/channel) was achieved in our experiment. It shows excellent channel spacing uniformity, and most of wavelength residuals are within $\pm$0.10 nm.

2. Principle

Fig. 1 shows the schematic of a sampled grating with π-equivalent phase shift (π-EPS) [11], [12]. The Bragg wavelengths of the $\pm 1^{st}$ subgratings, which are usually used as resonators, can be expressed as

$$\lambda_{\pm 1} = 2n_{\text{eff}}(\lambda_{\pm 1}) \frac{P\Lambda_0}{P \pm \Lambda_0}. \tag{1}$$

Therefore, for the REC technique, in order to obtain high channel uniformity, three issues including sampling pattern error, seed grating error and ERI error, have to be addressed.

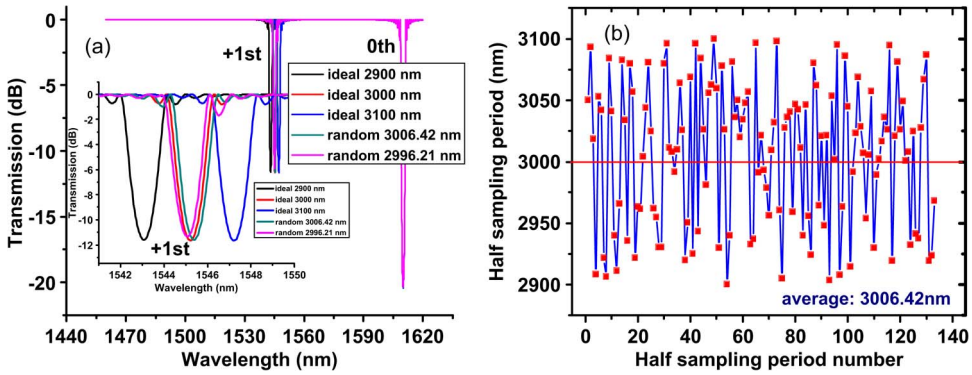

Fig. 2. (a) The transmission spectra for the sampled grating with ideal sampling structures (half sampling periods of 2900 nm, 3000 nm, and 3100 nm) and the sampling structures with random errors (mean half sampling periods of 3006.42 nm and 2996.21 nm). (b) The half sampling periods along the cavity with random errors with mean half sampling periods of 3006.42 nm.

2.1. The Sampling Random Error

According to the analysis in [11] and [12], the deviation in sampling period only leads to a much smaller deviation (smaller than 1/100 of the sampling period deviation) in the $\pm$1st sub-gratings. Moreover, if the statistical property of the sampling period error is considered, the $\pm$1st sub-grating errors will be further reduced [13]. The Bragg wavelength of a grating with random error is determined by the average Bragg grating period and the random error only leads to the broadening of the grating stop-band [14]. According to Central-limit theorem in probability theory, the sampling period error $(\bar{P}-\mu)/(\sigma/\sqrt{N})$ follows the Gaussian distribution and can be expressed as

$$\frac{\bar{P}-\mu}{\sigma/\sqrt{N}} \sim Gauss(\mu, \sigma^2/N) \tag{2}$$

where $\overline{P}$ denotes the mean value of the sampling periods $P(z)$ along cavity, μ is the expectation of sampling periods with random error, and σ is standard deviation. N is the number of sampling periods. From equation (2), we can see that standard deviation of $\overline{P}$ is equal to $\sigma/\sqrt{\mathrm{N}}$, and if we assume that sampling period distribution function $P(z)$ has expectation μ of 6 μm which is the exact sampling period that we want, the standard deviation σ of 50 nm, and the sampling number N of about 66 for a 400 μm long cavity, then we have that standard deviation of $\overline{P}$ is only 6.15 nm. Fig. 2(a) shows simulated transmission spectra for the sampled gratings with different sampling pattern random errors. As can be seen, the Bragg wavelengths for uniform sampling pattern with half period of 3000 nm, random sampling pattern with average half period of 3006.42 nm and average half period of 2996.21 nm are very close to each other. However, the random error in half sampling period is actually nearly up to $\pm$100 nm as is shown in Fig. 2(b) which describes the half sampling period distribution along the cavity of the gratings with average half period of 3006.42 nm. Since the process error of within $\pm$100 nm can be easily ensured using current fabrication technology, one can conclude that the wavelength error caused by sampling pattern is very insignificant.

As a result, the key factors to affect the channel spacing are the seed grating deviation and the inaccuracy of the ERI of waveguides, which will be analyzed in detail in following section.

2.2. Effect of the Seed Grating Period Error

During the holographic exposure for seed grating fabrication, the deviation of grating period usually occurs, which leads to nonuniform shifts in lasing wavelengths for different channels.

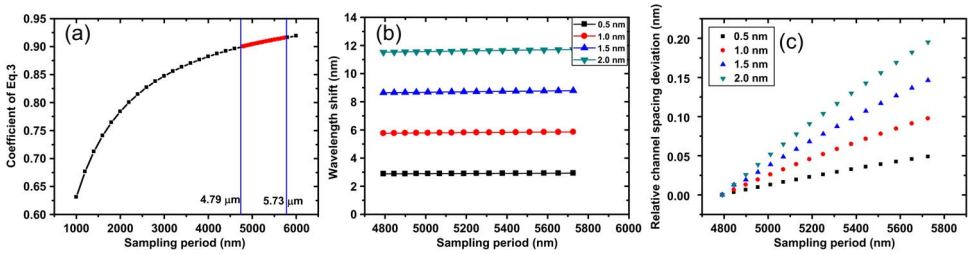

Fig. 3. (a) The plot of the coefficient $(P/(P+\Lambda_0))^2$ of (3) versus sampling period. Two points of 4.79 μm and 5.73 μm indicate the sampling period range that used in the array fabricated in our experiment. (b) The curves of wavelength shifts under different seed grating deviations (0.5 nm, 1.0 nm, 1.5 nm, and 2.0 nm). (c) The relative channel spacing deviations related to the smallest sampling period of 4790 nm according to Fig. 3(b).

The deviation of the $+1$st sub-grating period can be expressed as

$$\Delta\Lambda_{+1} = \left(\frac{\Lambda_{+1}}{\Lambda_0}\right)^2 \Delta\Lambda_0 = \left(\frac{P}{P+\Lambda_0}\right)^2 \Delta\Lambda_0. \tag{3}$$

Fig. 3(a) plots the curve of coefficient of (3) versus sampling period. Clearly in the region with large sampling period, the variation of the curve is small, which implies the wavelength deviation of each channel will approaches to the same for identical deviation of seed grating period. More specifically, if the sampling periods of a 16-channel DFB laser array varies from 4.79 μm to 5.73 μm, the corresponding wavelength shifts for different seed grating period deviation (0.5 nm, 1.0 nm, 1.5 nm, and 2.0 nm) can be calculated [see Fig. 3(b)]. Whilst the absolute wavelength of an individual channel in MLA is strongly affected by the seed grating error, the effect of seed grating deviation on channel spacing is much weaker. For example, if the seed grating has deviation of 2 nm, wavelength changes by around 12 nm [see Fig. 3(b)], the channel spacing, however, deviates only by no more than 0.2 nm as shown in Fig. 3(c). Therefore, if the fabrication of seed grating period is well controlled within 2.0 nm in deviation, high precision of wavelength spacing in MLAs can be achieved.

Indeed, our experiment showed that there is a difference of 0.48 nm between design and actual experimental measurement values in seed grating period, which translates to channel spacing error of no more than 0.05 nm. The error is so insignificant that can be neglected.

2.3. Effect of the Guided Mode Dispersion

Guided mode dispersion in an optical waveguide arises from the material dispersion and the waveguide dispersion [1]. The wavelength spacing can be expressed as

$$\Delta\lambda_{\text{actual}} = 2[n_2\Lambda_2 - n_1\Lambda_1]. \tag{4}$$

Here, Λ_1 and Λ_2 stand for different grating periods, n_1 and n_2 denote the two effective refractive indexes at wavelengths of λ_1 and λ_2, respectively. Due to the wavelength dispersion of the guided modes, the ERI of the two wavelengths can be expressed as

$$n_1 = n_0 + \Delta n_1 \quad \text{and} \quad n_2 = n_0 + \Delta n_2. \tag{5}$$

Here n_0 is the ERI around λ_0, which is used as the reference index. Δn_1 and Δn_2 are the differences in ERI between λ_0 and λ_1, λ_0 and λ_2 respectively. Inserting (5) into (4), one can have

$$\Delta\lambda_{\text{actual}} = 2[(n_0+\Delta n_2)\Lambda_2 - (n_0+\Delta n_1)\Lambda_1] = \Delta\lambda_{\text{design}} + 2(\Delta n_2\Lambda_2 - \Delta n_1\Lambda_1). \tag{6}$$

Apparently, there is an additional component $\Delta\lambda_{\text{offset}}$ in wavelength spacing, as shown in the following:

$$\Delta\lambda_{\text{offset}} = 2(\Delta n_2\Lambda_2 - \Delta n_1\Lambda_1). \tag{7}$$

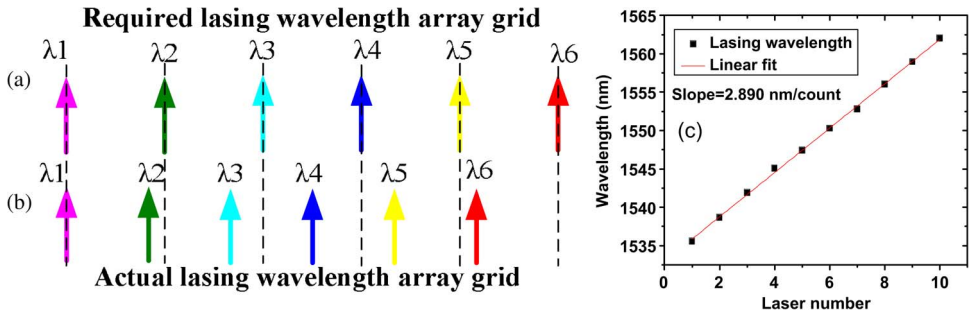

Fig. 4. The schematic of the wavelength spacing error caused by the incorrectly estimated ERI. (a) The required wavelength spacing; (b) the actual wavelength spacing with incorrectly estimated dispersion slope; (c) the measured lasing wavelength of a 10-wavelength MLA without dispersion compensation.

From (7), one can see that the wavelength spacing will be smaller than the actual one [see Fig. 4(a) and (b)], if the dispersion is not considered in design. In this paper, we refer to the dispersion effect as the "wavelength spacing shrink effect," and the shrink ratio can be expressed as follows:

$$\frac{\Delta\lambda_{\text{actual}}}{\Delta\lambda_{\text{design}}} = 1 + \frac{2(\Delta n_2\Lambda_2 - \Delta n_1\Lambda_1)}{\Delta\lambda_{\text{design}}}. \tag{8}$$

To confirm our theoretical analysis, we fabricated a 10-wavelength DFB laser array without dispersion compensation. The designed MLA has wavelength spacing of 3.2 nm and uniform ERI of 3.20. All the lasers were measured at identical injection current of 70 mA and same ambient temperature of 24 °C. No additional tuning was applied. The measured result is shown in Fig. 4(c) and the wavelength spacing is 2.890 nm after linear fitting. Therefore, the shrink ratio is 0.9031 which is consistent with the theoretical analysis above.

2.4. Measurement of the Guided Mode Dispersion

In order to measure the dispersion, a simple measurement method based on the Fabry–Pérot (F-P) modes for REC technique based laser is proposed here. A special feature of an REC based DFB laser is that it has potential to lase at the 0th grating order (λ_0) in small-gain region. But because the 0th-order lasing and the F-P are not dominant and almost cannot be observed in anti-reflection AR (< 1%) and anti-reflection AR (< 1%) coating configuration, instead, anti-reflection AR(1%) and high-reflection HR (90%) facet coating were used to enhance the 0-order round-trip feedback and F-P modes as is shown in Fig. 5 where the 0th lasing is around 1.502 μm. The actual grating period Λ_0 can be measured before regrowth during laser fabrication. Therefore, the ERI (n_0) at λ_0 can be calculated by Bragg condition. Then, the ERI of the nearest F-P mode (n_{FP0}) approximately equals n_0. According to the expression of the F-P mode, the index of other F-P modes can be determined successively.

The detailed procedure can be described as the following: (a) The ERI of the 0th Bragg wavelength was calculated by the measured grating period and the equation $n_0 = \lambda_0/2\Lambda_0$, as shown in Fig. 5. Here, Λ_0 is the measured grating period. (b) Find the F-P mode near the wavelength λ_0 and it is denoted as λ_m (shown in Fig. 5). Since the dispersion is rather small and the ERI difference between Bragg wavelength and the nearest F-P mode is also very small, $n(\lambda_m)$ approximately equals to n_0. Therefore, the order m of the F-P mode can be calculated by $L = m(\lambda_m/2n(\lambda_m))$. Here, L is the cavity length. (c) Find the next order F-P mode with wavelength of λ_{m-1}, the corresponding ERI can be expressed as $n(\lambda_{m-1}) = (\lambda_{m-1}/2L)(m-1)$. As a result, the whole effective refractive indexes of the F-P modes can be obtained. The dispersion slope can then be obtained by linear fitting.

One laser was measured under different test conditions and the results are show in Fig. 6. After linear fitting, the dispersion slope of around $-2.02e^{-4}$ nm^{-1} is obtained. It also shows that

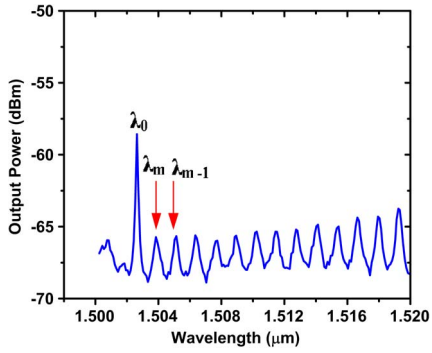

Fig. 5. The measured lasing spectrum around 0th-order Bragg wavelength of a REC based DFB laser.

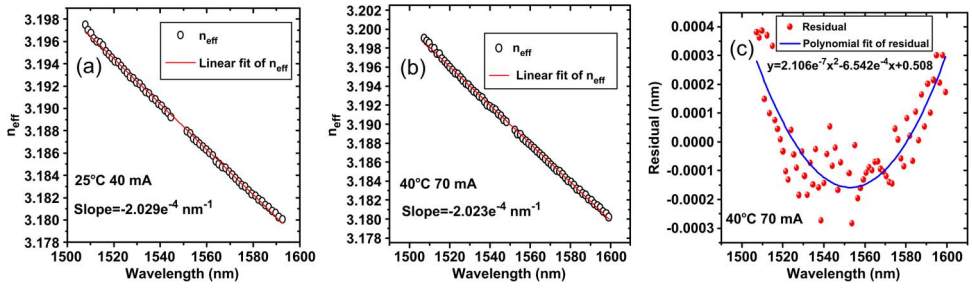

Fig. 6. (a) and (b) The measured dispersion slope under different test conditions. (c) Residuals of ERI after linear fitting at temperature of 40 °C and injection current of 70 mA.

the value maintains nearly identical for different injection currents and ambient temperatures which is quite helpful for the design since lasers are usually operated under different conditions. It is noticeable that some points around 1543 nm are unavailable, which is due to the main DFB mode is lasing here. Nevertheless, according to the F-P mode wavelength spacing (∼1.35 nm around 1550 nm in our experiment), the order m of the next F-P mode outside the DFB grating stop-band can still be easily determined.

The residual of the ERI after linear fitting is shown in Fig. 6(c). As it can be seen, a nonlinear component, though it is very small, in dispersion can be observed, The maximum residual is only about $4.0e^{-4}$ corresponding to a wavelength range from 1507 nm to 1525 nm. The relative index variation is about $-2.12e^{-5}$ nm^{-1} which is one order smaller than the linear dispersion slope. Therefore, the nonlinear component of the dispersion can be ignored.

Though the measured dispersion is considerably small, its effect on the wavelength spacing reduction for the MLAs with large wavelength coverage is significant. For example, the shrink ratios can be calculated by utilizing the measured dispersion slope of about $-2.0e^{-4}$ nm^{-1} and the reference index n_0 of 3.20 at the wavelength of 1491 nm. For the central wavelengths being around 1550 nm, the calculated shrink ratios with designed channel spacing of 0.4 nm, 0.8 nm, and 1.6 nm are 0.8994, 0.8994, and 0.8993, respectively.

3. Experimental Results of 16-Wavelength MLA

We designed and fabricated 16-wavelength DFB laser arrays based on REC technique with carefully evaluated waveguide dispersion and good seed grating precision. The fabrication was identical to the process used for conventional DFB semiconductor lasers, except that an additional step of photolithography for sampling pattern is needed. All laser materials were grown by a conventional two-stage lower-pressure metal-organic vapor phase epitaxy (MOVPE). The EPI structure which is grown on an n-InP substrate in the first epitaxial growth, consists of an InP

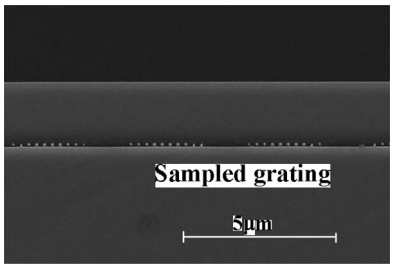

Fig. 7. The SEM picture of cross section of the fabricated DFB laser with sampled grating.

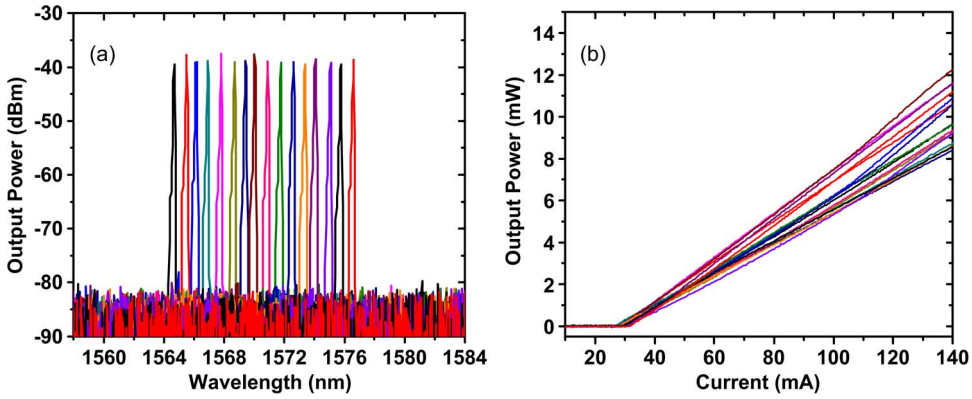

Fig. 8. (a) The measured spectra of 16-wavelength DFB laser array under the ambient temperature of 23 °C and injection current of 80 mA. (b) P-I curves of the laser array.

buffer layer, a lower optical confinement layer, a multiple-quantum-well (MQW) active structure and an upper optical confinement layer. The MQW structure contains five 6 nm thick and compressive-strained (1.2%) AlGaInAs wells separated by six 9 nm thick and tensile-strained (-0.45%) AlGaInAs barriers. The sampled grating for MLA was then patterned on the upper separate-confinement-heterostructure (SCH) layer by a conventional holographic exposure followed by a conventional photolithography. The designed seed grating period is 258.77 nm and the measured grating period is 259.25 nm. The sampling periods are from 4.79 μm to 5.73 μm. Fig. 7 shows the scanning electron microscope (SEM) picture of the fabricated sampled grating. The cavity length was 600 μm and the 2-μm ridge waveguide was used for all channels. AR($<$ 1.0%)/AR($<$ 1.0%) facet coating was applied to avoid the random facet phase.

The measured spectra of the16-wavelength DFB laser array are shown in Fig. 8(a). All the individual lasers are tested at the same conditions, i.e., the ambient temperature of 23 °C and injection current of 80 mA. Good SLM properties are achieved. Fig. 8(b) shows the power-current (P-I) curves of the array. The threshold currents are around 30 mA which is mainly attributed to long cavity (600 μm) and AR/AR coating. However, the threshold current can be improved by optimizing the laser structures such as employing buried heterostructure (BH) in which threshold currents is typically between 6 mA and 9 mA [15]. In order to analyze the wavelength spacing uniformity, we plot the lasing wavelengths and linear fitting is then made as is shown in Fig. 9(a). The wavelength residuals are also shown in Fig. 9(b). The slope, which means the wavelength spacing, is 0.7944 nm/channel with relative error being only 0.7%. The most wavelength residuals of all lasers are within $\pm$0.10 nm (One laser is -0.152 nm and another is -0.104 nm) which indicates excellent wavelength uniformity across the fabricated array. If the same uniformity was achieved for MLA based on EBL process, then the grating pitch deviation would have to be within around $\pm$0.031 nm, which is a tremendous challenge.

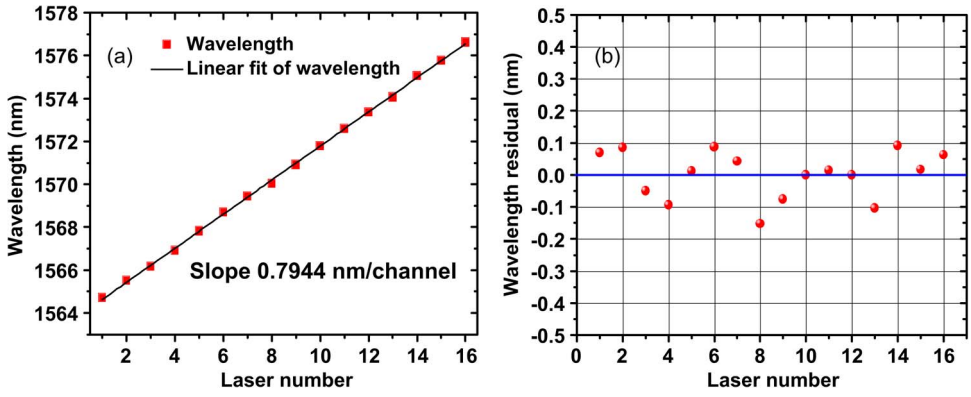

Fig. 9. (a) The measured lasing wavelengths of the laser array. (b) Wavelength residuals after linear fitting.

4. Discussion

As is shown above, the effect of the dispersion on the channel spacing is considerable. In this section, we give further discussions on the waveguide dispersion.

4.1. Error in Dispersion Estimation

In fact, obtaining the exact ERI at the Bragg wavelength (or the n_{eff} of the F-P mode around Bragg wavelength) and the cavity length L is always a challenge, because usually the grating periods are not same for different lasers (there may be up to 1.0 nm error in the fabrication) and there is random error in the laser cleavage too. Therefore, the effect of these errors on the dispersion slope is elaborately analyzed in this section.

4.1.1. The Reference ERI Error

According to above analysis, the dispersion slope can be approximated as a linear function of wavelength. So the error in reference refractive index only leads to a whole shift in the refractive index for a range of wavelengths without changing the dispersion slope. Therefore, if the index error is about 0.01 and the lasing wavelength of MLA is around 1550 nm, then the slope error is only about $6.45e^{-6}$ nm^{-1}, according to (A.6), which is two orders smaller than the dispersion slope.

It also indicates that it is reasonable to approximate the ERI of 0th DFB induced lasing wavelength to the one of the nearest F-P mode in the measurement method.

4.1.2. Cavity Length Error

The cavity length error L can be considered as the inaccurate estimation of the F-P mode order. According to (A.2), the slope error induced by cavity length error can be expressed as

$$\delta C_L = \frac{\delta m}{2L}. \tag{9}$$

For example, supposing $\delta L = 5.0$ μm, $n_{\text{eff}} = 3.20$; $L = 400.0$ μm and the resonant wavelength is around 1550 nm, the error is calculated to be $2.5806e^{-5}$ nm^{-1} which is about one order smaller than the dispersion slope. Usually this error is also small, but it can be further reduced by improving cleavage precision.

4.2. A Modified Dispersion Estimation Method

If the measured dispersion slope is still incorrect, the measured wavelength array grid will also be incorrect. We can measure the dispersion again to obtain a more accurate value.

However, the precision is probably still limited by the measurement conditions. Here, we propose another method to determine the dispersion with better precision based on the previously used dispersion value and the measured wavelength spacing. The designed wavelength spacing can be expressed as

$$\Delta\lambda_{\text{design}} = \lambda_2 - \lambda_1 = 2(n_0 + \Delta n_2)\Lambda_2 - 2(n_0 + \Delta n_1)\Lambda_1. \tag{10}$$

Then, the actually measured wavelength spacing can be expressed as

$$\Delta\lambda_{\text{actual}} = \lambda_2 - \lambda_1 = 2\left(n_0 + \Delta n_2 + \Delta n_2'\right)\Lambda_2 - 2\left(n_0 + \Delta n_1 + \Delta n_1'\right)\Lambda_1. \tag{11}$$

Here, Δn_1 and Δn_2 are the index compensation values used for the first time design. Since one still cannot obtain the correct ERI or the required wavelength spacing, so some additional index differences, $\Delta n_1'$ and $\Delta n_2'$ should be applied for actual values. Λ_2 and Λ_1 are the actual grating periods for two different wavelengths. Then, the actual wavelength spacing can be further expressed as

$$\begin{aligned}\Delta\lambda_{\text{actual}} &= 2\left(n_0 + \Delta n_2 + \Delta n_2'\right)\Lambda_2 - 2\left(n_0 + \Delta n_1 + \Delta n_1'\right)\Lambda_1 \\ &= 2(n_0' + \Delta n_2)\Lambda_2 - 2\left(n_0' + \Delta n_1\right)\Lambda_1 + 2\left(\Delta n_2' - \Delta_n'\right)\Lambda_2 \\ &\approx \Delta\lambda_{\text{design}} + 2\left(\Delta n_2' - \Delta n_2'\right)\Lambda_2. \end{aligned} \tag{12}$$

Here, $n_0' = n_0 + \Delta n_1'$.

Because the dispersion can be considered as linear function of wavelength, according to the above measurement results and the value of $\Delta n_1'$ being pretty small, the approximation in the formula derivation of (12) can be implemented. Then, $2(\Delta n_2' - \Delta n_1')\Lambda_2$ can be considered as the error caused by the inaccurately estimated dispersion value. Its value can be expressed as

$$\Delta n_2' - \Delta n_1' = \frac{\Delta\lambda_{\text{actual}} - \Delta\lambda_{\text{design}}}{2\Lambda_2}. \tag{13}$$

Therefore, the corrected dispersion slope C_{new} can be expressed as

$$C_{\text{new}} = \frac{(n_2 - n_1)}{\Delta\lambda_{\text{actual}}} = \frac{\Delta n_2 - \Delta n_1 + \Delta n_2' - \Delta n_1'}{\Delta\lambda_{\text{actual}}}. \tag{14}$$

From (12)–(14), if the measured wavelength spacing, designed wavelength spacing and the grating period Λ_2 are determined, the dispersion slope can be corrected. Here, we give an example in the following.

We initially design the wavelength spacing of 0.8 nm with two wavelengths of 1550.8 nm and 1550.0 nm, and the designed dispersion slope is $-2.0e^{-4}$ nm^{-1}. Assuming the ERI around 1491 nm is 3.20, the grating periods of two wavelengths can be fixed according to the estimated dispersion slope. If the actually measured wavelength spacing is 0.7680 nm corresponding to a shrink ratio of 0.96, we can find out the value of $\Delta n_2' - \Delta n_1'$ using (13). Therefore, the corrected dispersion slope is $-2.9399e^{-4}$ nm^{-1} according to (14). In order to further verify this method, we use the newly corrected dispersion and the fixed grating periods to calculate the wavelength spacing, the calculated value is about 0.7619 nm which has reduced the relative error to be 0.795%. In contrast, the relative error by using the original dispersion value of $-2.0e^{-4}$ nm^{-1} is about 4.17%. Therefore, the error is highly reduced by the modified dispersion measurement method. The residual error is caused by the approximation of $\Delta\lambda$ design in (12). Nevertheless, we can loop this procedure again by a new experiment using the previously calculated dispersion value to make the dispersion further approach the real one.

4.3. Thermal Crosstalk

As shown in [16]–[18], the thermal cross talk occurs under simultaneous operation of the lasers in MLA. As a result, the lasing wavelengths can be influenced mutually with wavelength

shift ratio of about 0.1 nm/°C. Some methods may be applied in the future to reduce the thermal crosstalk such as reducing the thickness of the chip to increase the heat conduction from active region to heat sink and etching the deep trench for air gap between two adjacent lasers [19].

5. Conclusion

The channel spacing uniformity of MLA based on REC technique is theoretically studied in detail. It is found that the dispersion of the guided mode can significantly affect the channel spacing while the seed grating period deviation mainly shift the whole lasing wavelengths in the array. By carefully designing the sampling pattern with dispersion effect being included and ensuring high precision processing of seed grating period, excellent results of lasing wavelength spacing with channel spacing of 0.7944 nm/channel (designed value of 0.80 nm/channel) and the most wavelength residuals within $\pm$0.1 nm have been experimentally achieved.

Appendix A

The reference ERI error is analyzed in the following section.

The resonant modes in F-P cavity can be expressed as

$$n_m = m\frac{\lambda_m}{2L}. \tag{A.1}$$

The dispersion slope around λ_m can be expressed as

$$C = \frac{n_{m+1} - n_m}{\lambda_{m+1} - \lambda_m} = \frac{m}{2L} + \frac{\lambda_{m+1}}{2L(\lambda_{m+1} - \lambda_m)}. \tag{A.2}$$

Applying (A.1) to (A.2), we can have

$$C = \frac{n_m}{\lambda_m} + \frac{\lambda_{m+1}}{2L(\lambda_{m+1} - \lambda_m)}. \tag{A.3}$$

Because the dispersion can be approximated as linear function of wavelength, the index can be expressed as

$$n_m \approx n_n + C(\lambda_m - \lambda_n). \tag{A.4}$$

Therefore, the error of refractive index in different order modes can be expressed as

$$\delta n_m = \delta n_n. \tag{A.5}$$

Then, the error in dispersion can be expressed as

$$\delta C_n \approx \frac{\delta n_m}{\lambda_m} = \frac{\delta n_n}{\lambda_m}. \tag{A.6}$$

References

[1] T.-P. Lee *et al.*, "Multiwavelength DFB laser array transmitters for ONTC reconfigurable optical network testbed," *J. Lightw. Technol.*, vol. 14, no. 6, pp. 967–976, Jun. 1996.

[2] H. Zhu *et al.*, "The fabrication of eight-channel DFB laser array using sampled gratings," *IEEE Photon. Tech. Lett.*, vol. 22, no. 5, pp. 353–355, Mar. 2010.

[3] J. Zhao *et al.*, "Experimental demonstration of a 16-channel DFB laser array based on nanoimprint technology," *Semicond. Sci. Technol.*, vol. 28, no. 5, pp. 1–6, Apr. 2013.

[4] W. Li, X. Zhang, and J. Yao, "Experimental demonstration of a multi-wavelength distributed feedback semiconductor laser array with an equivalent chirped grating profile based on the equivalent chirp technology," *Opt. Exp.*, vol. 21, no. 17, pp. 19 966–19 971, Aug. 2013.

[5] C. Zhang, H. Zhu, S. Liang, L. Han, and W. Wang, "Monolithically integrated 4-channel-selectable light sources fabricated by the SAG technology," *IEEE Photon. J.*, vol. 5, no. 4, Aug. 2013, Art. ID. 1400407.

[6] M. G. Young *et al.*, "Wavelength uniformity in λ/4 shifted DFB laser array WDM transmitters," *Electron.Lett.*, vol. 31, no. 20, pp. 1750–1752, Sep. 1995.

[7] T. Kjellberg, S. Nilsson, T. Klinga, B. Broberg, and R. Schatz, "Investigation on the spectral characteristics of DFB lasers with different grating configurations made by electron-beam lithography," *J. Lightw. Technol.*, vol. 11, no. 9, pp. 1405–1415, Sep. 1993.
[8] D. Jiang, X. Chen, Y. Dai, H. Liu, and S. Xie, "A novel distributed feedback fiber laser based on equivalent phase shift," *IEEE Photon. Technol. Lett.*, vol. 16, no. 12, pp. 2598–2600, Dec. 2004.
[9] Y. Dai and X. Chen, "DFB semiconductor lasers based on reconstruction-equivalent-chirp technology," *Opt. Exp.*, vol. 15, no. 5, pp. 2348–2353, Mar. 2007.
[10] Y. Dai and J. Yao, "Numerical study of a DFB semiconductor laser and laser array with chirped structure based on the equivalent chirp technology," *IEEE J. Quantum Electron.*, vol. 44, no. 10, pp. 938–945, Oct. 2008.
[11] Y. Shi *et al.*, "Experimental demonstration of eight-wavelength distributed feedback semiconductor laser array using equivalent phase shift," *Opt. Lett.*, vol. 37, no. 16, pp. 3315–3317, Aug. 2012.
[12] Y. Shi *et al.*, "Study of the multiwavelength DFB semiconductor laser array based on the reconstruction-equivalent-chirp technique," *J. Lightw. Technol.*, vol. 31, no. 20, pp. 3243–3250, Oct. 2013.
[13] Y. Shi, R. Liu, S. Liu, and X. Zhu, "A low-lost and light-wavelength-precision fabrication method for multiwavelength DFB semiconductor laser array," *IEEE, Photon. J.*, vol. 6, no. 3, pp. 1–12, Jun. 2014.
[14] G. Coppola, A. Irace, A. Cutolo, and M. Iodice, "Effect of fabrication errors in channel waveguide Bragg gratings," *Appl. Opt.*, vol. 38, no. 9, pp. 1752–1758, Mar. 1999.
[15] J. Li *et al.*, "An eight-wavelength BH DFB laser array with equivalent phase shifts for WDM systems," *IEEE Photon. Technol. Lett.*, vol. 26, no. 16, pp. 1593–1596, Aug. 2014.
[16] L. Han *et al.*, "Temperature characteristics of monolithically integrated wavelength-selectable light sources," *Chin. Phys. Lett.* vol. 30, no. 10, Jun. 2013, Art. ID. 108501.
[17] L. Ma, H. Zhu, M. Chen, C. Zhang, and W. Wang, "InGaAsP/InP DFB laser array monolithically integrated with MMI combiner and SOA," *Proc. SPIE,* vol. 8552, Nov. 2012, Art. ID. 85520F.
[18] T. Hayashi, K. Sato, and S. Sekine, "Thermal interaction in a distributed-feedback laser diode (DFB LD) array module," *J. Lightw. Technol.*, vol. 11, no. 3, pp. 442–447, Mar. 1993.
[19] A. Fred *et al.*, "Method of operating an array of laser sources integrated in a monolithic chip or in a photonic integrated circuit (PIC)," U.S. Patent 7 079 720 B2, Jan. 10, 2005.